Jurnal Ilmiah Teknik Elektro Komputer dan Informatika (JITEKI)
Vol. 9, No. 3, September 2023, pp. 511-521
ISSN: 2338-3070, DOI: 10.26555/jiteki.v9i3.26272

Circuit Modeling of Dual Band MIMO Diversity Antenna for LTE and X-Band Applications

Aminu Gambo A [1], S. F. Kolawale [2], Sani Saminu [3], Ali Danladi [4], Adamu Halilu Jabire [5]
[1] National Museums and Monument Kano, Nigeria
[2] Nigeria Defence Academy Kaduna, Nigeria
[3] Department of Biomedical Engineering, University of Ilorin, Ilorin, Nigeria
[4] Institute of Space Science and Engineering, Abuja, Nigeria
[5] Taraba State University, Department of Electrical and Electronics Engineering

INFO

Article history:

Received May 24, 2023
Revised July 02, 2023
Published July 11, 2023

Keywords:

Multiple-input-multiple-output (MIMO) antennas;
Equivalent circuit model;
Isolation;
Defective ground structure (DGS)

ABSTRACT

This paper presents a study on developing a dual-band antenna equivalent circuit model for X-Band and LTE applications. MIMO antennas play a crucial role in modern wireless communication systems, and understanding their impedance behavior is essential. This work proposes a dual-band lumped equivalent circuit model, utilizing gradient optimization based on antenna-simulated S-parameters in Advanced Design System (ADS). The four radiating elements of the MIMO antenna are accurately modeled, considering their geometry and the defected ground structure (DGS) effect, which enhances the antenna's isolation and low correlation coefficient (ECC). The calculated lumped equivalent circuit model is validated through rigorous simulation and measurement data, demonstrating consistency with the expected results. The experimental measurements show measured isolation exceeding 20 dB while achieving a maximum realized gain of 5.9 dBi and an efficiency of 87%. The developed model holds promise for improving the design and performance of MIMO antennas for various applications.

Corresponding Author:

Adamu Halilu Jabire, Taraba State University, Department of Electrical and Electronics Engineering
Email: adamu.jabire@tsuniversity.edu.ng

1. INTRODUCTION

Antennas play a crucial role in wireless communication by radiating guided waves into free space, enabling global connectivity. To achieve the desired coverage for long-distance transmission, a single omnidirectional antenna is often insufficient [1]. Multiple directional antennas and arrays are required to obtain the appropriate radiation pattern and gain. Antenna arrays offer advantages such as increased overall gain, diversity reception, interference elimination, and improved Signal Noise Ratio (SINR) [2]. However, the practical implementation of many antenna elements in base stations and mobile terminals is limited by physical space constraints. Moreover, complex antenna configurations with multiple resonances pose challenges in developing accurate equivalent circuit models [3], [4], [5]. Equivalent circuit models can be used to understand antenna performance better. An electrical model like this can simulate the circuits required to analyze planar antennas. It isn't easy, however, to develop equivalent circuits for complex antenna configurations with many resonances [6]. Equivalent circuit models, such as transmission lines and lumped circuits, have been widely used to improve antenna design capabilities. Researchers have explored various techniques, such as using metamaterials [7]. Split-ring resonators (SRR), meandered lines, and different configurations of radiating elements address issues like electromagnetic suppression, isolation improvement, and mutual coupling reduction in MIMO antennas [8], [9]. The authors in [10] reported a MIMO antenna in which the elements were placed perpendicular to reduce the electromagnetic interaction, but the antenna design is complex. In [11], a MIMO antenna was configured using split-ring resonators (SRR) and meandered lines for isolation improvement. The reported antenna has a good isolation characteristic, but it is bulky. [12] reported a two-port

MIMO antenna with low mutual coupling and pattern diversity; however, the antenna is a single-band MIMO antenna but has excellent performance. In [13], a researcher presented a monopole antenna with a partial ground plane and metamaterials for 5G sub 6GHz applications, the antenna has good results in terms of impedance width and MIMO metric performances, but it is not a self-decoupled antenna. [14], proposed an orthogonal arrangement of radiated elements to increase isolation. The design technique is complex. Authors in [15] used an electromagnetic band gap structure to reduce the mutual coupling. The electromagnetic suppression technique used is complex. The author in [16] employed a protruded ground structure to improve the isolation of the antenna, but the antenna is not compact. An RFID parasitic antenna was modeled as a parallel RLC circuit in [17]. The disadvantage of this antenna is its single configuration and single band. A study in [18] shows that a series of parallel RLC circuits can be used to construct an equivalent circuit model of a small multiband antenna. The antenna has a multiband characteristic but is not a MIMO antenna. In [19], researchers present a new method to determine the ultra-wideband lumped equivalent circuit of a four-port circular monopole antenna using the gradient optimization method in ADS. The mutual coupling technique was not self-decoupled. [20], provides a method for generating a super wideband electrical model of frequency reconfigurability. The authors used PIN-Diodes to configure in either the ON or OFF state, with an additional rejected band. A single antenna was used instead of MIMO. [21] proposed an equivalent circuit modeling using frequency domain data from simulation or measurements. The authors used a single antenna, not MIMO.

This paper aims to design and realize L-shaped dual-band frequencies for LTE and X-Band applications. The proposed antenna's frequency domain response is rationally optimized based on antenna design and substrate characteristics, leading to the development of an accurate circuit model. The derived circuit is simulated using ADS software, and its accuracy is verified by comparing it with the antenna's simulation results. A self-decoupled technique was used for mutual coupling reduction. This article outlines the MIMO antenna configuration and working principles in Section 2, then presents an equivalent circuit model and antenna analysis. Section 3 discusses the experimental results and MIMO metric performance, and finally, Section 4 concludes the paper. By addressing the specific challenges of dual-band frequencies and considering rational optimization techniques, this research contributes to advancing antenna design for LTE and X-Band applications.

2. MIMO ANTENNA CONFIGURATION

The geometry of the proposed MIMO antenna for dual-band applications, including LTE and X band, is shown in Fig. 1. The antenna consists of four L-shape radiators arranged in an orthogonal manner, as evident in Fig. 1. The MIMO antenna is excited via a 50Ω microstrip feedlines. Cutting slots of various shapes in the ground plane can change the surface current distribution. Such slotted geometry is known as defected ground structure (DGS). The DGS technique is employed in this work to achieve dual band frequency responses and improve low mutual coupling between the MIMO antenna. The proposed antenna is etched on top of an FR4 substrate with a loss tangent of 0.025, a relative permittivity of 4.4, and a thickness of 1.6mm. Computer simulation technology (CST) and advanced design system (ADS) were used to optimize the antenna's performance, and Table 1 lists the optimized parameters.

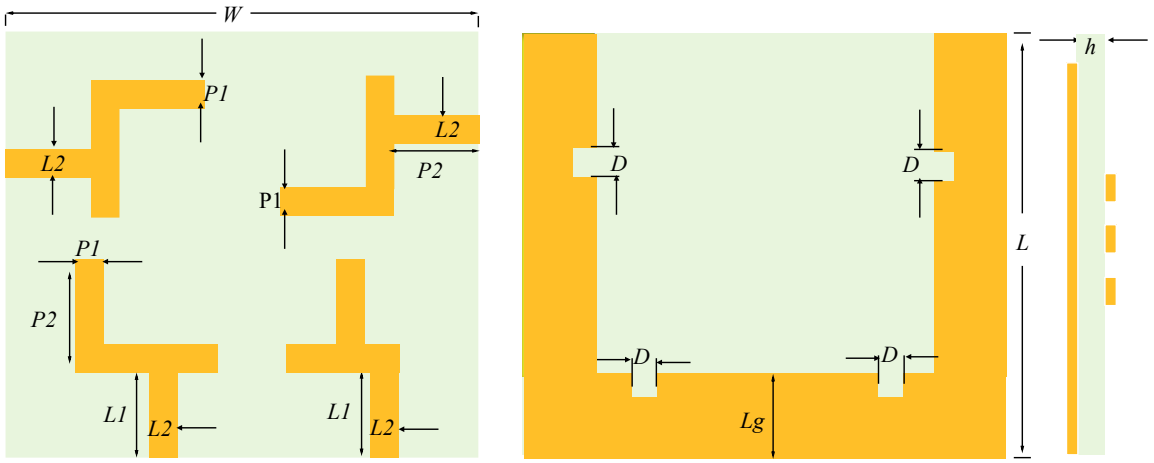

Fig. 1. Schematic view of the MIMO system; (a) Front view, (b) Back view, (c) Side view.

Table 1. Dimensions of the proposed MIMO antenna

Parameter	Size (mm)	Parameter	Size (mm)
D	4	L_g	10
L	60	P_1	3
L_1	11.05	P_2	10
L2	3	W	60

2.1. Equivalent Circuit Model Analysis

The proposed dual-band MIMO antenna's equivalent circuit was optimized using the ADS software, as evident in Fig. 2. The analysis was to validate the simulated results from CST. The analysis used the four-port impedance termination, four series inductors, and four parallel RLC components. Each of the parallel RLCs represents a single monopole antenna. Three control engines were also set up: the s-parameter for a range of frequencies from 1 – 12GHz, the optimization engine where a type of optimization can be selected and finally, the goal engine where the limit of values for each component can be set. In this work, the simulation variable setup for all the components was from minimum to maximum. The gradient optimization method was chosen because of its computational efficiency and produced a stable error gradient and convergence [21]. A dual frequency response is achieved after the circuit simulation, which produces the LTE and X band applications compared to CST full wave simulation. It is evident in Fig. 3. The optimized circuit components are R1 = 36.22Ω, R2 = 314844Ω, R3 = 242040Ω, R4 = 43498Ω, L1 = 28.1nH, L2 = 3.09nH, L3 = 1466.9nH, L4 = 1467.5nH, C1 = 18.60pF, C2 = 1.42pF, C3 = 1.5960pF, C4 = 2.3188pF, La = 220.6nH, Lb = 33820nH, Lc = 1.00nH, Ld = 129.34nH.

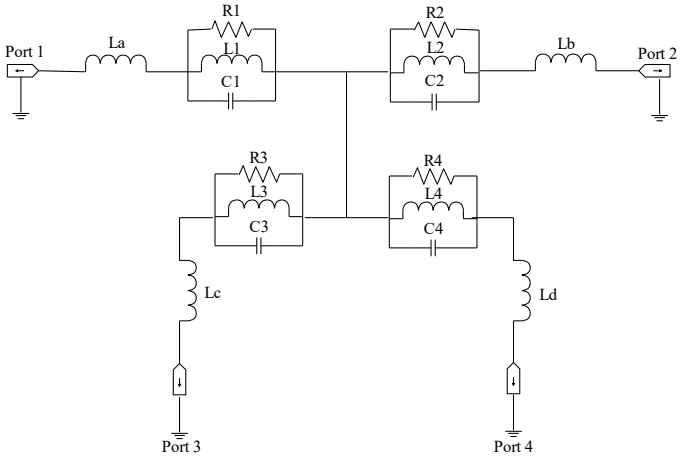

Fig. 2. The circuit model for the MIMO antenna.

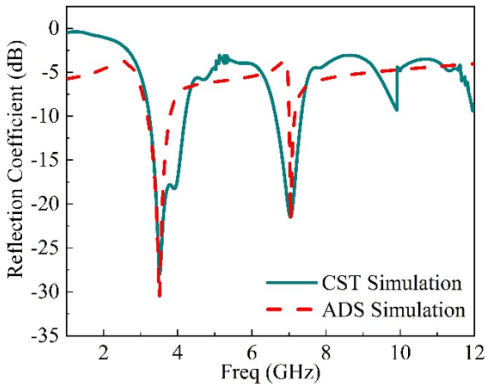

Fig. 3. S11 of the equivalent circuit model.

2.2. Circuit model parametric analysis

A parametric optimization was performed on several circuit components to see their effect on the antenna response. Varying the value of the input inductance 'La' affects the antenna at the highest frequencies above 6 GHz. The “La” values of 292.6pH, 300.4pH, 353.6pH and 399.0pH are visualized in Fig. 4(a). Decreasing 'La'

yields the S11 dual-band range, with an optimal value of 220.6 pH. The second component examined is "C4". The effect is shown in Fig. 4(b). This affects the higher frequencies of 7GHz. The value of resistor "R1" is also examined, as depicted in Fig. 4(c); the effect is on the two resonant frequencies. Note that increasing the resistance increases the frequency response accordingly.

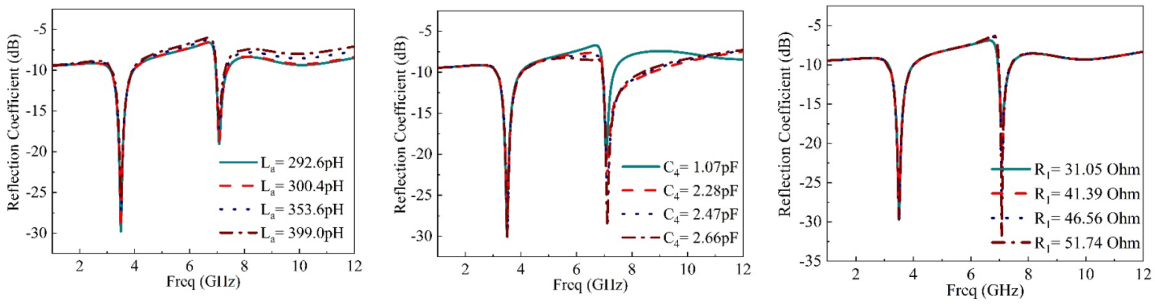

(a) (b) (c)

Fig. 4. Optimization of the circuit components (a) inductance, (b) capacitance, (c) resistance.

3. RESULTS AND DISCUSSION

3.1. Scattering parameters

The suggested MIMO antenna's simulated and measured results are presented in this section. Fig. 5a depicts the experimental setup, while Fig. 5b depicts the MIMO antenna prototype. A vector network analyzer was used to test and measure the S11 spectra and isolation performance of the MIMO antenna (Agilent network analyzer N3242C). An anechoic chamber was used to measure the far-field pattern after some calibrations. The reception antenna used was a common horn antenna, with a 1m gap between the test antenna and the reference antenna. Fig. 6-Fig. 8 shows the proposed MIMO antenna's S11, S21 spectra, gain, and radiation efficiency. The measured and simulated S11 spectra are at 3.5GH z and 7GHz. The measured and simulated S21 spectra are < -20dB, with a peak realized gain of 5.9dBi and radiation efficiency of 87%. The results from simulation and measurement are in good agreement.

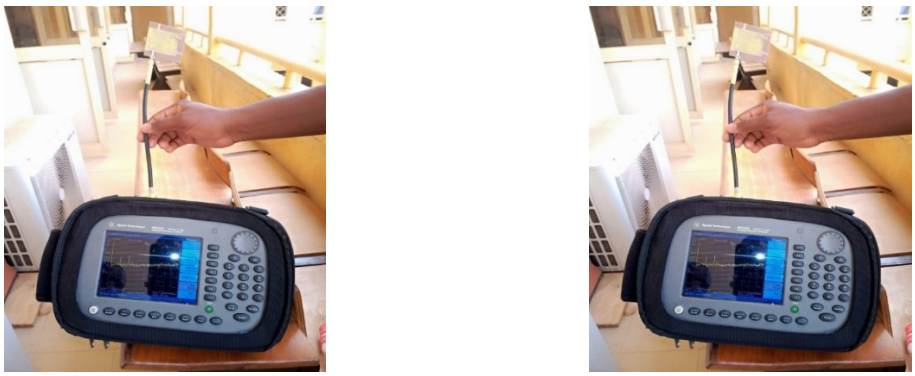

(a) (b)

Fig. 5. (a) Prototype, (b) The measurement setup.

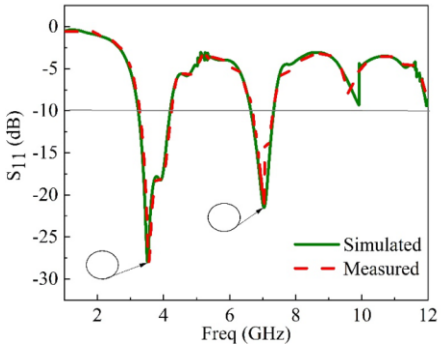

Fig. 6. The contrast of simulated and measured S11.

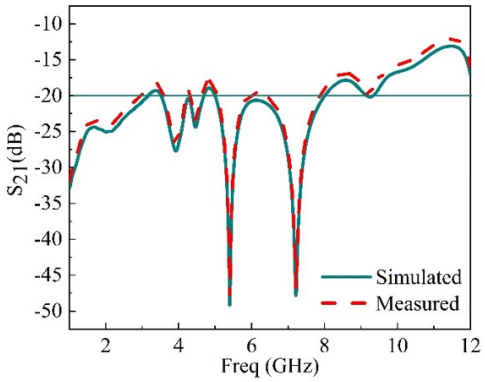

Fig. 7. The contrast of simulated and measured S21.

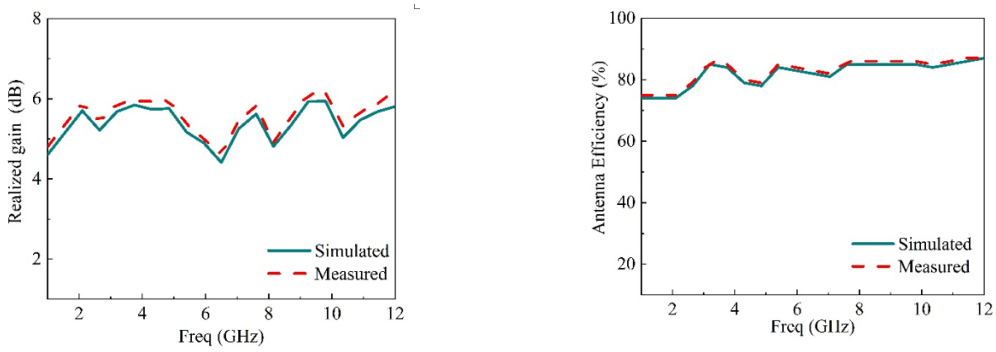

(a) (b)

Fig. 8. The contrast of simulated and measured results (a) peak gain (b) efficiency.

3.2. Far-field pattern and surface current

The MIMO antenna was measured in a calibrated anechoic chamber to validate the simulated far-fields. The fabricated prototype was placed on a turntable in front of a broadband horn antenna at a distance of 1m apart. Fig. 9(a-b) displays measurements and simulations of the far-field pattern at 3.5GHz and 7GHz, respectively. The pattern shows an omnidirectional behavior at a lower frequency of 3.5GHz (receiving signals equally from all directions), while a near-omnidirectional pattern is depicted at a higher frequency of 7GHz. There are some distortions in measured results due to soldering and other technical issues during the measurement. The surface current density for the proposed MIMO antenna has been investigated when both ports 1 to 4 are excited. Fig. 10-Fig. 11 depicts the current distribution at 3.5GHz and 7GHz, respectively. An exciting port has a higher concentration of currents. Much of the currents were concentrated at the feedline and the main radiator.

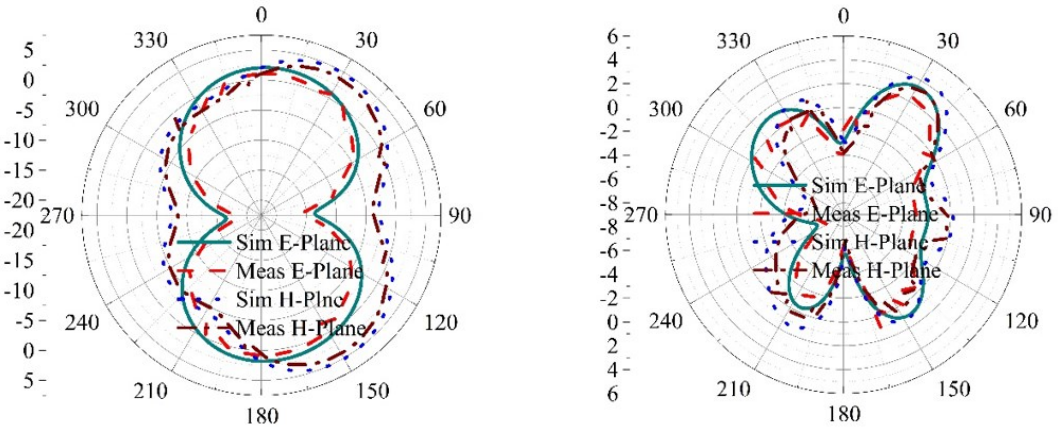

(a) (b)

Fig. 9. The simulated and measured 2D far-field pattern (a) 3.5GHz, (b) 7GHz.

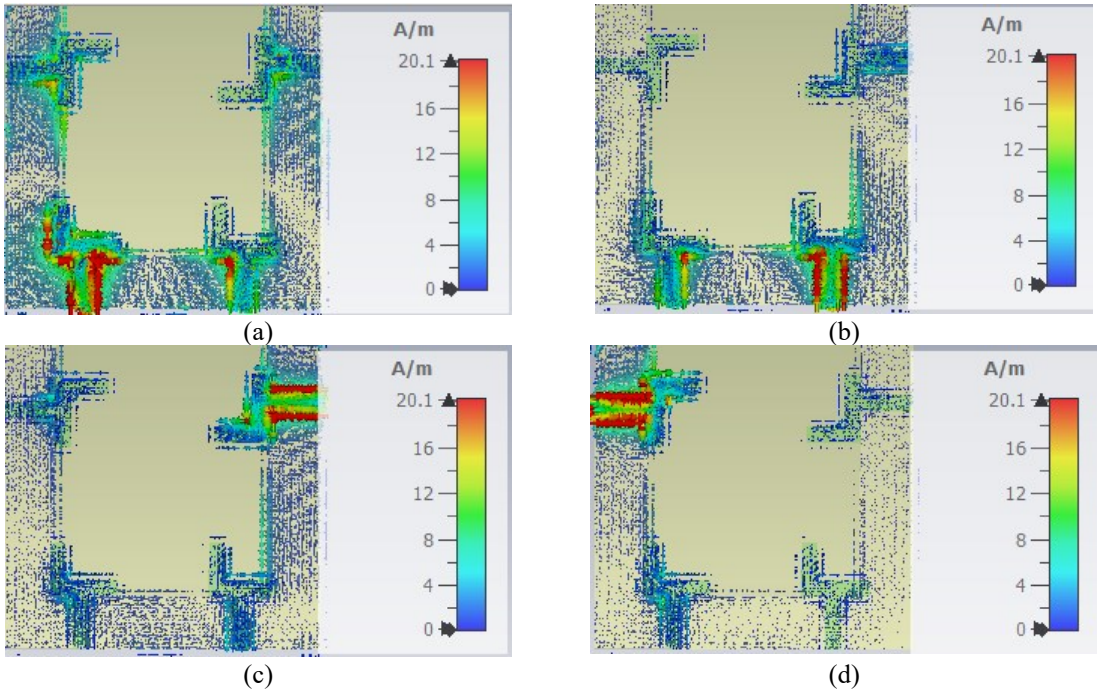

Fig. 10. Current distribution at 3.5GHz when a different port is excited (a) port 1, (b) port 2, (c) port 3, (d) port 4.

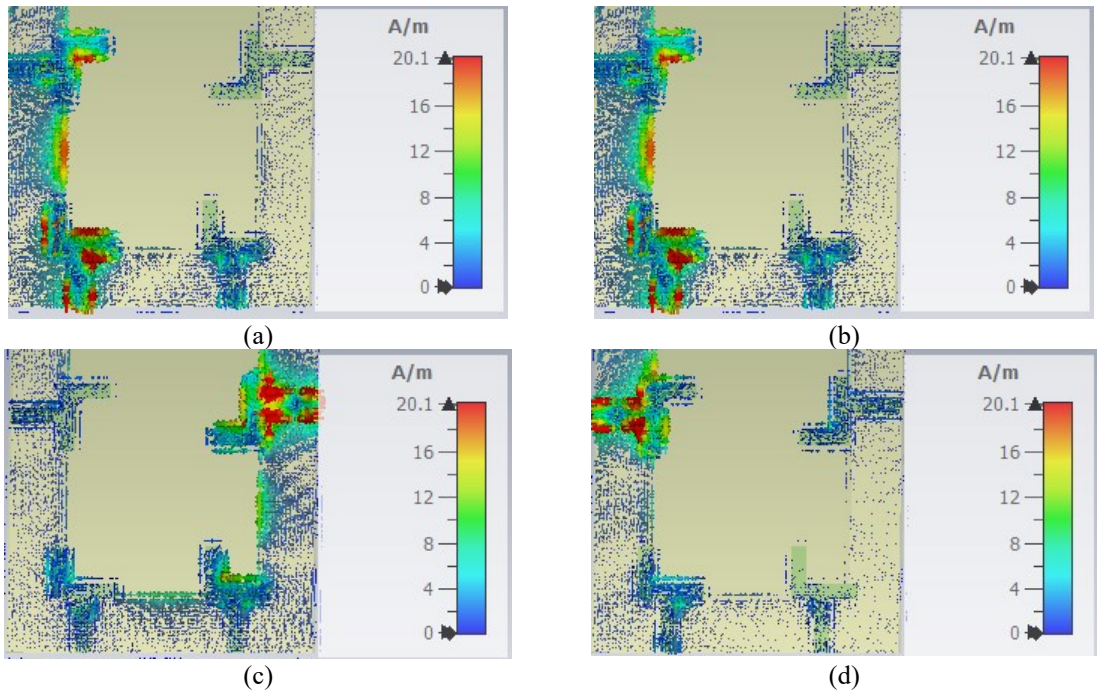

Fig. 11. Current distribution at 7GHz when a different port is excited (a) port 1, (b) port 2, (c) port 3, (d) port 4.

3.3. MIMO Metric Performance

The diversity performance of the proposed antenna has been analyzed and discussed in this section. The proposed MIMO antenna's total active reflection coefficient (TARC), Channel capacity loss (CCL), correlation coefficient, diversity gain, and the MIMO antenna's mean effective gain. The parameter that quantifies signal interference between MIMO channels (TARC) is computed using the following expression [22], [23], [24], [25], [26].

$$TARC = \frac{\sum_{n=1}^{N}|b_i|^2}{\sum_{n=1}^{N}|a_i|^2} = \sqrt{\frac{\left(S_{ii}+S_{ij}\right)^2+\left(S_{jj}+S_{ji}\right)^2}{n}} \quad (1)$$

In MIMO, ai denotes the incident wave from one port to another, bi denotes the reflected wave from one port to another, and n refers to the number of MIMO elements at both ends. TARC also gives information about the perceptible return loss of the MIMO antenna. The simulated and measured TARC is depicted in Fig. 12, which is less than -10 dB.

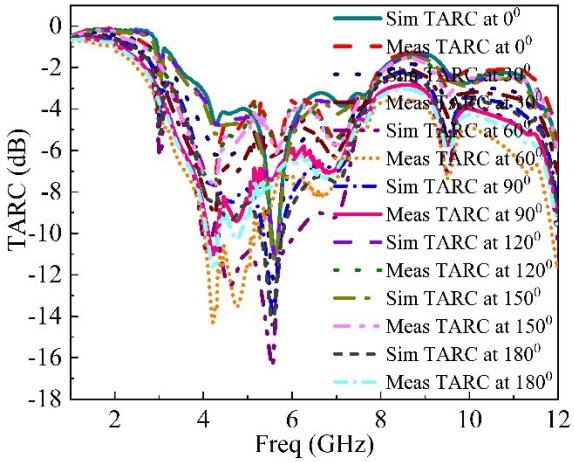

Fig. 12. Measured and simulated total active reflection coefficient.

The envelope correlation coefficient determines how well an antenna's elements correlate. It affects the channel capacity of the MIMO system. According to the standard, ECC should be less than 0.1 [27] [28]. The ECC variation is shown in Fig. 13, with a value of less than 0.0012. It can be evaluated using (2) [29].

$$\rho_e = \frac{\left|\iint_{4\pi}\left[\vec{F}_1(\theta,\varphi)\times\vec{F}_2(\theta,\varphi)d\Omega\right]\right|^2}{\left|\iint_{4\pi}\left[\vec{F}_1(\theta,\varphi)\right]\right|^2 d\Omega\left|\iint_{4\pi}\left[\vec{F}_2(\theta,\varphi)\right]\right|^2 d\Omega} \quad (2)$$

The $\vec{F}_i(\theta,\varphi)$ stands as the far-field property of the MIMO when port 1 or 2 is excited. The diversity gain is another performance metric for verifying the degree of power reduction that is transmitted; it is computed from the ECC by using the following (3) [30], [31]. The proposed antenna's DG is 9.994dB, as illustrated in Fig. 14.

$$DG = 10\times\sqrt{1-{\rho_e}^2} \quad (3)$$

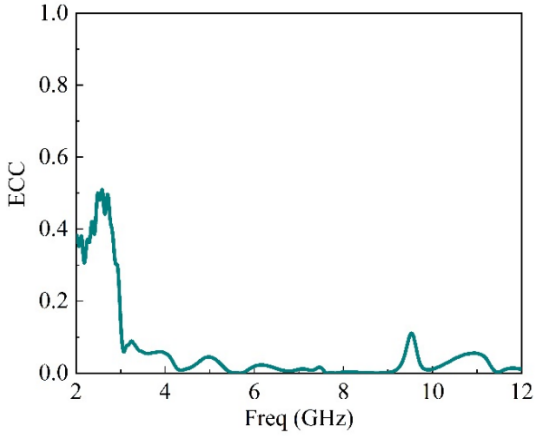

Fig. 13. Variation of ECC with frequency.

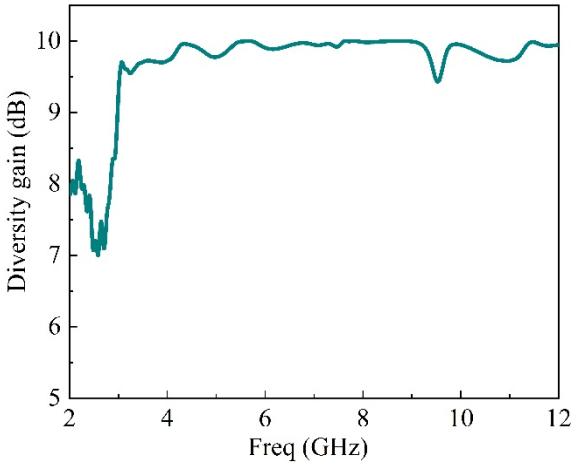

Fig. 14. Variation of DG with frequency.

A linear channel capacity loss results from an increase in antenna elements. Increased antenna components offer improved channel capacity, and a lower CCL is a crucial need for MIMO systems to manage actual data rates well. As shown in Fig. 15, the measured and simulated CCL can be calculated using (4)–(5) [32], [33], 34].

$$CCL = -log_2(A^\rho) \tag{4}$$

$$A^\rho = \begin{vmatrix} \rho_{11} & \rho_{12} \\ \rho_{21} & \rho_{22} \end{vmatrix} \tag{5}$$

An effective gain is a parameter that measures how much power is received through the diversity antenna compared to the sum of the average power received through the isotropic antenna [35],[36]. Mean effective gain is calculated from (6) [37], [38], [39], [40]. Fig. 16 shows the plotted result of the MEG. Table 2 compares various aspects of the proposed MIMO antenna with other relevant studies available in the literature. In comparison to [2], [3], [9], [10], [23], [27], and [29], the proposed work is compact, has high gain, high efficiency, and is highly isolated.

$$\text{Mean Effective gain } = 0.5\left[1 - \sum_{j=1}^{N}\left|S_{ij}\right|^2\right] \tag{6}$$

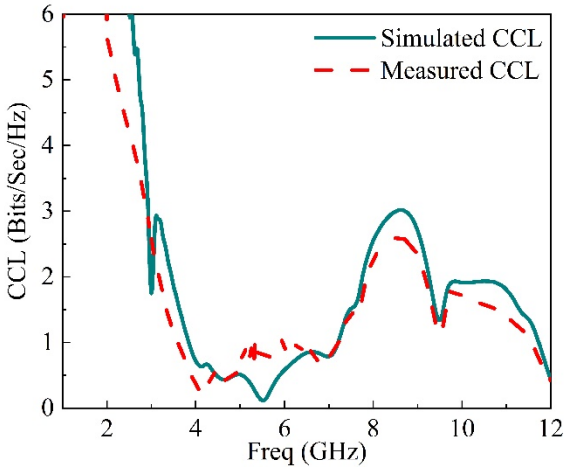

Fig. 15. Measured and simulated antenna's CCL.

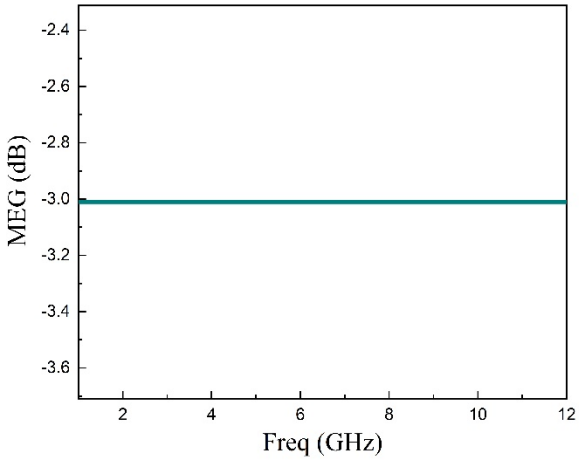

Fig. 16. Variation of MEG with frequency.

Table 2. Comparison of the proposed design with prior literature

Ref.	Dimensions (mm)	Substrate	Peak gain (dBi)	Efficiency (%)	ECC
[2]	66×66	FR-4	>3	85	<0.01
[3]	67×139	FR-4	-	-	<0.001
[9]	43×26	FR-4	4.21	-	<0.1
[10]	150×75	FR-4	4.6	80	<0.07
[14]	30×35	Rogers R04350B	8.3	82	<0.01
[23]	40×40	TMM4 Laminate	3.5	89	<0.4
[27]	39×30	Rogers 5880	5.8	-	<0.02
[29]	85×85	FR-4	2.9	70	<0.0006
This work	60×60	FR-4	5.9	87	<0.001

4. CONCLUSION

The dual-band MIMO antenna has been successfully demonstrated for LTE and X-band applications. The dual-band can be configured using an L-shape radiator and a defective ground structure. To validate the MIMO antenna, an equivalent circuit model has been introduced. The diversity performance has been experimentally verified, and it is excellent in terms of TARC, ECC, DG, CCL and MEG. The proposed MIMO antenna has an efficiency of 87% and an overall gain of 5.9dBi. The dual-band performance of the antenna makes it a suitable candidate for wireless communication devices. Future work will employ another technique to achieve more multiband frequencies for 5G sub 6GHz applications.

REFERENCES

[1] H. Sudarsan, R. Gayathri, and V. Sittallut, "Investigation of compact dual port octagonal MIMO antenna with triple-band rejection capabilities with good isolation," *Turkish Journal of Computer and Mathematics Education*, vol. 12, no. 10, pp. 4987-5000, 2021, https://doi.org/10.17762/turcomat.v12i10.5267.

[2] I. Adam, M. N. M. Yasin, N. Ramli, *et al*., "Mutual coupling reduction of a wideband circularly polarized microstrip antenna," *IEEE Access,* vol. 7, pp. 97838-97845, 2019, https://doi.org/10.1109/Access.2019.2928899.

[3] M Nada, A. Khalil, A. S. Oras, *et al*., "A design of MIMO prototype in C-Band frequency for future wireless communications," *Advanced Electromagnetics*, vol. 9, no. 1, pp. 1-7, 2020, https://doi.org/10.7716/aem.v9i1.1333.

[4] S. Zheng, X. Chen and G. F. Pedersen, "Mutual coupling suppression with decoupling ground for massive MIMO antenna arrays," *IEEE Transaction on Vehicular Technology*, vol. 68, no. 8, pp. 7273-7282, 2019, https://doi.org/10.1109/TVT.2019.2923338.

[5] E. Fritz-Andrade, A. Perez-Miguel, R. Gomez-Villanueva and H. Jardon-Aguilar, "Characteristic mode analysis was applied to reduce the mutual coupling of a four-element patch MIMO antenna using a defective ground structure," *IET Microwave Antenna and Propagation*, vol. 14, no. 2, pp. 215- 226, 2020, https://doi.org/10.1049/iet-map.2019.0570.

[6] J. Yousaf, H. Jung, K. Kim, W. Nah, "Design, analysis, and equivalent circuit modeling of dual-band PIFA using a stub for performance enhancement," *J. Electromagn. Eng. Sci,* vol. 16, pp. 169-181, 2016, https://doi.org/10.5515/JKIEES.2016.16.3.169.

[7] A. H. Jabire, H. Zheng, and A. Abdu, "Split rectangular loop resonator inspired MIMO monopoles for GSM/LTE/WLAN applications," *Journal of Communications,* vol. 14, no. 6, pp. 511-517, 2019, https://doi.org/10.12720/jcm.14.6.511-517.
[8] A. Khan, S. Bashir, S. Ghafoor, K. K. Qureshi, "Mutual coupling reduction using ground stub and EBG in a compact wideband MIMO antenna," *IEEE Access,* vol. 9, pp. 40972-40979, 2021, https://doi.org/10.1109/Access.2021.3065441.
[9] A. K. Panda, S. Sahu, R. K. Mishra, "A compact dual-band 2×1 metamaterial inspired MIMO antenna system with high port isolation for LTE and WIMAX applications," *Int. J. RF Microw Comput Aided Eng*., vol. 27, e21122, 2017, https://doi.org/10.1002/mmce.21122.
[10] O. P. Naser, J. B. Haleh, I. A. Yasir, *et al*., "Ultrawideband diversity MIMO antenna system for the future mobile handset," *Sensors*, vol. 20, pp. 1-19, 2020, https://doi.org/10.3390/s20082371.
[11] L. Sun, Y. Li, Z. Zhang, H. Wang, "Self-decoupled MIMO antenna pair with shared radiator for 5G smartphones," *IEEE Trans. Antenna Propag*., vol. 68, pp. 3423-3432, 2020, https://doi.org/10.1109/TAP.2019.2963664.
[12] A. Iqbal, A. Altaf, M. Abdullahi, M. Alibakhshikenari, *et al*., "Modified U-shaped resonator as decoupling structure in MIMO antenna," *Electronics*, vol. 9, p. 1321, 2020, https://doi.org/10.3390/electronics9081321.
[13] A. H. Jabire, H. Zheng, A. Abdu, Z. Song, "Characteristic mode analysis and design of wideband MIMO antenna consisting of metamaterial unit cell," *Electronics*, vol. 8, no. 68, pp. 1-14, 2019, https://doi.org/10.3390/electronics8010068.
[14] M. Khalid, S. Iffat-Neqvi, M. Rahman, *et al*., "Four-port MIMO antenna with a defected ground structure for 5G millimeter-wave applications," *Electronics*, vol. 9, no. 71, 2020, https://doi.org/10.3390/electronics9010071.
[15] N. Jaglan, S. D. Gupta, E. Thakur, *et al*., "Triple band-notched mushroom and uniplanar EBG structure-based UWB MIMO/diversity antenna with enhanced wideband isolation," *Int. J. Electron Commun*, vol. 90, pp. 36-44, 2018, https://doi.org/10.1016/j.aeue.2018.04.009.
[16] J. D. S. Wang and J. Mo, "Design of a twelve-port MIMO antenna system for multi-mode 4G/5G smartphone applications based on characteristic mode analysis," *IEEE Access*, vol. 8, pp. 90751-90759, 2020, https://doi.org/10.1109/Access.2020.2994068.
[17] A. Ferchich, M. K. Azizi, G. Ali, "Analysis of a square parasitic antenna using lumped elements," *Int. J. Electron. Telecommun*, vol. 58, pp. 279-283, 2012, https://doi.org/102478/v10177-012-0039-x.
[18] L. Akrou, O. Aghzout, H. J. A. da Silva, M. Essaidi, "Design of a compact multiband antenna with band rejection features for mobile broadband satellite communications," *Prog. Electromagn. Res. C*, vol. 68, pp. 95-106, 2016, https://doi.org/10.2528/PIERC16073103.
[19] A. H. Jabire, S. Sani, S. Saminu, M. J. Adamu, M. I. Hussein, "A crossed polarized four port MIMO antenna for UWB communication," *Heliyon*, vol. 9, pp. 1-15, 2022, https://doi.org/10.1016/j.heliyon.2022.e12710.
[20] Y. Fauri, S. Ahmad, S. Naseer, K. Alhammami, *et al*., "Compact super-wideband frequency diversity hexagonal shaped monopole antenna with switchable rejection band," *IEEE Access*, vol. 10, pp. 42321-42333, 2022, https://doi.org/10.1109/Access.2022.3167387.
[21] Y. Kim, H. Ling, "Equivalent circuit modeling of broadband antennas using a rational function approximation," *Microw. Opt. Technol. Lett*, vol. 48, pp. 950-953, 2006, https://doi.org/10.1002/mop.21529.
[22] J. C. Dash, and D. Sarkar, "A four-port CSRR-loaded dual-band MIMO antenna with suppressed higher order modes," *IEEE Access*, vol. 10, pp. 30770 – 30777, 2022, https://doi.org/10.1109/Access.2022.3160831.
[23] S. Ahmad, S. Khan, B. Manzoor, *et al*., "A compact cpw-fed ultra-wideband multi-input-multi-output (MIMO) antenna for wireless communication networks," *IEEE Access*, vol. 10, pp. 25278 – 25289, 2020, https://doi.org/10.1109/Access.2022.3155762.
[24] M. Capek, L. Jelinek and M. Masek, "Finding optimal total active reflection coefficient and realized gain for lossy multiport antennas," *IEEE Transaction on Antennas and Propagation*, vol. 69, no. 5, pp. 2481 – 2493, 2021, https://doi.org/10.1109/TAP.2020.3030941.
[25] R. Yadav, C. Gotra, V. S. Pandey and S. Kumar, "Graphene-based two port MIMO yagi-uda antenna for THz applications," *Micro and Nanostructures*, vol. 181, pp. 1-11, 2023, https://doi.org/10.1016/j.micrna.2023.207616.
[26] K. Muthukrishnan, M. M. Kamaruzzaman, L. Sunil, and S. Vishal, "Superlative split ring resonator shaped ultra-wideband and high gain 1×2 MIMO antenna for terahertz communication," Nano Communication Networks, vol. 36, pp. 1-12, 2023, https://doi.org/10.1016/j.nancom.2023.100437.
[27] G. Saxena, S. Chintakindi, M. A. Kasim, *et al*., "Metasurface inspired wideband high isolation THz MIMO antenna for nano communication including 6G applications and liquid sensors," *Nano Communication Networks*, vol. 34, pp. 1-10, 2022, https://doi.org/10.1016/j.nancom.2022.100421.
[28] A. Iqbal, A. Smida, A. J. Alazani, *et al*., "Wideband circularly polarized MIMO antenna for high data wearable biotelemetric devices," *IEEE Access*, vol. 8, pp. 17935-19944, 2020, https://doi.org/10.1109/Access.2020.2967397.
[29] G. Saxena, S. Chintakindi, M. A. Kasim, *et al*., "Metasurface inspired wideband high isolation THz MIMO antenna for nano communication including 6G applications and liquid sensors," *Nano Communication Networks*, vol. 34, pp. 1-10, 2022, https://doi.org/10.1016/j.nancom.2022.100421.
[30] S. H. Ghadeer, S. K. A. Rahim, M., Alibakhshikenari, *et al*., "An innovative fractal monopole MIMO antenna for modern 5G applications," *Int. J. Electron. Commun*, vol. 159, pp. 1-16, 2023, https://doi.org/10.1016/j.aeue.2022.154480.

[31] A. Mohanty, and S. Sahu, "A micro four port THz MIMO antenna for nano communication networks," *Photonic and Nanostructures Fundamentals and Applications*, vol. 53, pp. 1-14, 2023, https://doi.org/10.1016/j.photonics.2023.101092.
[32] M. M. Kartha, M. Jayakumar, "Circularly polarized stub loaded annular ring patch antenna for 2×2 MIMO satellite application," *Measurement*, vol. 217, pp. 1-12, 2023, https://doi.org/10.1016/j.measurement.2023.113044.
[33] A. Abbas, N. Hussain, M. A. Sufian, *et al*., "Highly selective multiple notched UWB-MIMO antenna with low correlation using an innovative parasitic decoupling structure," *Engineering Science and Technology, an International Journal*, vol. 43, pp. 1-12, 2023, https://doi.org/10.1016/j.jestch.2023.101440.
[34] S. Karimulla, V. Kumar, "Diversity performance of band-notched ultra-wideband MIMO antenna," *Optic*, vol. 272, p. 170128, 2022, https://doi.org/10.1016/j.ijleo.2022.170128.
[35] S. Luo, D. Wang, Y. Chen, *et al*., "A compact dual port UWB-MIMO antenna with quadruple band-notched characteristics," *Int. J. Electron. Commun*, vol. 136, p. 153770, 2021, https://doi.org/10.1016/j.aeue.2021.153770.
[36] V. Puri, H. S. Singh, "Design of isolation improved MIMO antenna using Metasurface based absorber for wireless applications," *Optik-International Journal for Light and Electron optics*, vol. 259, pp. 1-11, 2022, https://doi.org/10.1016/j.ijleo.2022.168963.
[37] B. V. Nikam, M. R. Jadhav, "A compact quad-port band-notched MIMO antenna for WIMAX application with low mutual coupling," *Progress in Electromagnetic Research C.*, vol. 104, pp. 53-67, 2021, https://doi.org/10.2528/PIERC20060602.
[38] S. Anand, R. Theetharappan, "Metamaterial and SIW inspired isolating fences for lateral decoupling in MIMO antenna," *International Journal of Electronics and Communication*, vol. 166, pp. 1-13, 2023, https://doi.org/10.1016/j.aeue.2023.154667.
[39] S. H. Ghadeer. S. K. A. Rahim, M. Alibakhshikenari, *et al*., "An innovative fractal monopole MIMO antenna for modern 5G application," *International Journal of Electronics and Communication*, vol. 159, pp. 1-16, 2023, https://doi.org/10.1016/j.aeue.2022.154480.
[40] P. Sharma, R. N. Tiwari. P. Singh and B. K. Kanaujia, "Dual-band trident shaped MIMO antenna with a novel ground plane for 5G applications," *International Journal of Electronics and Communication*, vol. 155, pp. 1-11, 2022, https://doi.org/10.1016/j.aeue.2022.154364.